Analysis of a film-forming amine response in impedance spectra

Deni Jero, Nicolas Caussé, Éric Dantras, Aurélien Roggero, Thierry Buffeteau, Nadine Pébère

Analysis of a film-forming amine response in impedance spectra

Deni Jero[1,2*], Nicolas Caussé[1*], Eric Dantras[3], Aurélien Roggero[4], Thierry Buffeteau[5], Nadine Pébère[1]

[1]Université de Toulouse, CIRIMAT, UPS/INPT/CNRS, ENSIACET 4, Allée Emile Monso-CS 44362, 31030 Toulouse cedex 4, France

[2]ODYSSEE Environnement-Service R&D, Belle Croix, 72510 Requeil, France

[3]Université de Toulouse, Physique des Polymères, CIRIMAT, Université Paul Sabatier, Bât. 3R1b2, 118 Route de Narbonne, 31062, Toulouse Cedex 9, France

[4]Université de Lyon, INSA Lyon, UCBL, CNRS, IMP UMR 5223, 69621 Villeurbanne, France

[5]Université de Bordeaux, ISM, UMR 5255 CNRS, 351 Cours de la Libération, 33405 Talence, France

*Corresponding authors:

deni.jero@toulouse-inp.fr (D. Jero)

nicolas.causse@toulouse-inp.fr (N. Caussé)

Highlights

Abstract

Keywords

1. Introduction

Industrial plants from boilers to secondary circuits of nuclear pressurized water reactors, mainly constituted of carbon steel, are prone to corrosion. Film-forming amines (FFA) have been used for several decades, in addition to chemical water conditioning, to assure a satisfactory protection of the carbon steel surfaces [1]. FFA adsorb onto metallic surface and/or surface oxides by their amino group(s) while their alkyl chain points outwards limiting the aggressive species, such as oxygen, water and ions (Cl^-, SO_4^{2-}) to reach the surface; thus, reducing the corrosion processes [1][2].

Several aspects of FFA behavior must be investigated in order to achieve the optimum utilization of these molecules. In addition, there is no continuous and *in situ* measurement system for the analysis of FFA onto the industrial circuit surfaces. The *in situ* analysis of nanometric organic layers is technically and scientifically challenging, and even more on rough surfaces. Electrochemical impedance spectroscopy (EIS) stands out as one of the few techniques enabling the analysis of the inhibitive properties [3][4][5][6] and more recently, the determination of thin organic layer thicknesses adsorbed onto rough metallic surfaces [2][7]. In our recent work [8], N-oleyl-propanediamine (OLDA) adsorption kinetics onto carbon steel surface has been examined for two temperatures (25 °C and 50 °C) by using *in situ* EIS measurements. Furthermore, the adsorbed OLDA layer onto the steel surface has been characterized as a function of immersion time and temperature by *ex situ* Raman spectroscopy and polarization modulation infrared reflection absorption spectroscopy (PM-IRRAS) analysis. It has been found that in a 200 $mg.kg^{-1}$ NaCl neutral electrolyte, the OLDA adsorption and the corrosion kinetics of the carbon steel surface occurred simultaneously from 2 min of immersion and both phenomena intensified with increasing immersion time and temperature up until the stabilization of the electrochemical system. *Ex situ* surface analysis

suggested that OLDA adsorbs heterogeneously onto the steel surface and mixed OLDA/corrosion products layers were formed. The estimated thicknesses varied between 4 nm and 20 nm depending on the immersion time and temperature in agreement with the previous work of Baux *et al*. [2][7] concerning octadecylamine (ODA). This previous study allowed a methodology, combining *in situ* EIS and *ex situ* PM-IRRAS and Raman spectroscopy techniques, to be proposed for monitoring the OLDA adsorption kinetics onto rough surfaces in corrosive electrolytes.

The present work aims to further analyze the OLDA response in EIS to clarify its dielectric contribution in the overall metal (carbon steel)/OLDA/solution response as a function of immersion time and temperature. First, the dielectric response of "bulk" OLDA (without any electrolyte) was analyzed by broadband dielectric spectroscopy (BDS). This technique is generally used to study dielectric properties of polymers [9][10] and more recently to investigate the dielectric properties of Self-Assembled Monolayers (SAM) [11]. Then, PM-IRRAS analysis of the adsorbed OLDA onto the carbon steel surface for three temperatures (25 °C, 50 °C and 75 °C) were conducted to determine the thickness and the molecules organization. Finally, the impedance spectra of the carbon steel/OLDA/solution system were analyzed within the scope of OLDA dielectric and molecular structure properties. Thusly, the adsorbed OLDA layer initially formed onto the carbon steel surface at 25 °C, in a deaerated alkaline solution, in order to strongly limit the corrosion processes of the carbon steel, was further analyzed during temperature variations [25 °C ; 75 °C] based on the methodology proposed by Roggero *et al*. [12] for the study of molecular mobility of polymer based anticorrosive coatings by using EIS. The complex capacitance and conductivity formalisms were used to study the signature of the adsorbed OLDA onto the carbon steel surface from the impedance spectra.

2. Experimental

2.1. Materials

P265GH carbon steel cylindrical rods were supplied from SMB (France). Its chemical composition in weight percent is reported in Table 1. For the EIS measurements, the lateral part of the steel rod was covered with a heat-shrinkable insulating sheath, leaving only the tip of the carbon steel (surface area of 1 cm^2) in contact with the solution. Prior to the experiments, the electrode was polished with SiC paper (grade 1200), rinsed with deionized water and dried.

Table 1

Chemical composition (wt. %) of the P265GH carbon steel.

Element	C	Mn	Si	Cu	Cr	Al	Fe
wt. %	0.14	1.03	0.22	0.05	0.04	0.04	Bal.

For the PM-IRRAS analysis, disks of 1 cm^2 and 2 mm thick were cut from the carbon steel rod. The substrates were polished up to 0.25 μm with diamond paste and then with Al_2O_3 suspension. Afterwards, they were ultrasonically cleaned with ethanol, dried and exposed to UV-ozone for 15 min in order to remove organic impurities. Finally, they were fixed to the rotating disk electrode to reproduce the hydrodynamic conditions used for the EIS experiments.

N-oleyl-1,3-propanediamine (OLDA) with a purity of 98 % was supplied by ODYSSEE Environnement. OLDA was analysed in two forms: as bulk product (as-received) by differential scanning calorimetry (DSC) and by BDS and as adsorbed molecules onto a carbon steel surface by *ex situ* PM-IRRAS and *in situ* EIS.

2.2. Electrolytical solution

The OLDA adsorbed layer onto carbon steel was prepared from the immersion of the metal surface in a solution containing OLDA at a concentration of 100 $mg.kg^{-1}$. The pH of the solution was adjusted at 11 by adding NaOH (0.1 M). The chosen experimental conditions are close to those encountered in industrial water/steam circuit and strongly limit the corrosion processes of the carbon steel. The same experimental conditions were used for the PM-IRRAS analyses.

2.2. Differential Scanning Calorimetry (DSC)

DSC measurements, conducted with a Q2000 calorimeter, manufactured by TA Instruments, were used to investigate phase transitions of OLDA "bulk". A mass of approximately 10 mg of OLDA, previously stored at 40 °C, was put in a standard sealed aluminium pan. Three temperature ramps were applied (cooling, heating, cooling) in the temperature domain [-40 °C ; 60°C] at 20 $°C.min^{-1}$ under helium flow.

2.3. Broadband Dielectric Spectroscopy (BDS)

BDS measurements were performed isothermally in the temperature range [-150 ; 50 °C] with a temperature step of 5 °C using a Novocontrol BDS 4000 impedance analyzer and a commercial interdigitated electrode (Novocontrol-BDS 1410-20-150). Preliminary experiments of the adsorbed OLDA onto the interdigitated electrode from an aqueous solution containing 100 $mg.kg^{-1}$ of OLDA at a $pH_{25°C}$ = 11 (by analogy with the EIS methodology) did not yield an exploitable signal due to the too small quantity of adsorbed molecules. Therefore, OLDA was deposited into the interdigitated electrode in such a way that the interdigits were fully filled.

A sinusoidal voltage ($U^*(\omega, T)$) (700 mV of amplitude) was applied in the frequency

range [10^6 Hz;10^{-2} Hz] inducing a current ($I^*(\omega,T)$) out of phase with the applied voltage. The complex impedance is the ratio between the applied voltage and the measured current (Eq. 1).

$$Z^*(\omega,T) = \frac{U^*(\omega,T)}{I^*(\omega,T)} \quad \textbf{(1)}$$

The complex capacitance ($C^*(\omega,T)$) of the interdigitated electrode is related to the complex impedance according to Eq. 2.

$$Z^*(\omega,T) = \frac{1}{i\omega C^*(\omega,T)} \quad \textbf{(2)}$$

The complex capacitance ($C^*(\omega,T)$) of the interdigitated electrode therefore considers contributions from the substrate of the electrode ($\varepsilon^*_{su}(\omega,T)$) as well as the analyzed material ($\varepsilon^*_m(\omega,T)$) according to Eq. 3. C_0 refers to the capacitance of the interdigitated electrode.

$$C^*(\omega,T) = C_0(\varepsilon^*_{su}(\omega,T) + \varepsilon^*_m(\omega,T)) \quad \textbf{(3)}$$

The complex capacity and conductivity, used for the interpretation of the data, were calculated according to Eq. 4 and Eq. 5, respectively.

$$C^*(\omega) = C'(\omega) + iC''(\omega) = \frac{-Z''(\omega)}{\omega\left[(Z'(\omega))^2+(Z''(\omega))^2\right]} + i\frac{Z'(\omega)}{\omega\left[(Z'(\omega))^2+(Z''(\omega))^2\right]} \quad \textbf{(4)}$$

$$\sigma^*(\omega) = \sigma'(\omega) + i\sigma''(\omega) = \frac{\delta}{A}\left\{\frac{Z'(\omega)}{\left[(Z'(\omega))^2 + (Z''(\omega))^2\right]} + i\frac{-Z''(\omega)}{\left[(Z'(\omega))^2 + (Z''(\omega))^2\right]}\right\} \quad \textbf{(5)}$$

Where $C'(\omega)$ and $C''(\omega)$ are the real and imaginary parts of capacitance, respectively, the σ' (ω) and σ" (ω) are the real and imaginary parts of conductivity, respectively, Z' (ω) and Z" (ω) are the real and imaginary parts of the impedance modulus, respectively, A is the surface area of the electrode, and δ is the thickness of the OLDA adsorbed layer.

The complex capacitance and conductivity values were directly calculated by the Windeta software associated with the BDS apparatus.

2.4. Polarization Modulation Infrared Reflection Absorption Spectroscopy (PM-IRRAS)

PM-IRRAS experiments of OLDA deposited onto the carbon steel substrates for three temperatures (25 °C, 50 °C and 75 °C) were performed on a ThermoNicolet Nexus 670 FTIR spectrometer equipped with a PM-IRRAS optical bench (incidence angle of 75°), following the experimental procedure previously described [13]. The resolution was 4 cm^{-1} and the acquisition time 4 h. The PM-IRRAS spectra were calibrated in order to be presented in IRRAS units [14][15]. The thickness of the deposited OLDA was estimated according to the methodology described in our previous work [8].

2.5. Electrochemical Impedance Spectroscopy (EIS)

EIS measurements were performed with a Biologic VSP-245 apparatus with a conventional three-electrode cell. The working electrode consisted of the carbon steel rod. A Red-Rod reference electrode (saturated KCl) by Radiometer Analytical was used. The counter-electrode was a large platinum grid. The working electrode rotation rate was fixed at 500 rpm. The temperature of the solution was controlled by a water circulating bath which allowed an accuracy of ± 1 °C over the range [25 °C ; 75 °C]. The EIS measurements were conducted in a deaerated solution by using a sealed electrochemical cell. Prior to the carbon steel immersion, the solution was deaerated for 15 min by argon gas bubbling in a separated vial. Then, the solution was transferred to the electrochemical cell where an argon flux was maintained during the measurements. To further limit oxygen arrival, an oxygen scavenger was added to the solution. In this study, N, N-Diethylhydroxylamine (DEHA) at a concentration of 26 $mg.kg^{-1}$ was used based on its use as hydrazine substituent in industrial water/steam circuits [16].

The protocol applied for analyzing the metal/OLDA/solution response in EIS as a function of time and temperature is illustrated in Fig. 1.

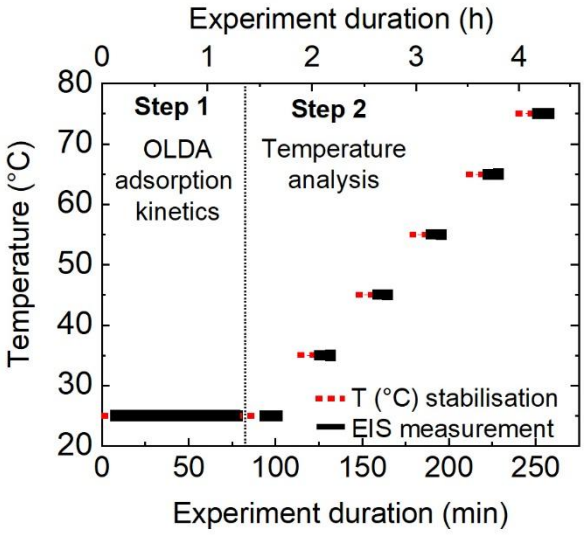

Fig. 1 Schematic diagram of the experimental protocol: a) OLDA adsorption kinetics onto the carbon steel surface monitored by EIS [8] and b) metal/OLDA/solution electrochemical response analysis during temperature variations.

Upon the contact between the carbon steel surface (already positioned into the electrochemical cell) and the solution containing 100 $mg.kg^{-1}$ of OLDA, the OLDA adsorption kinetics was followed (Step 1 in Fig. 1). The impedance spectra were recorded from 20 s of immersion and every 140 s for a total duration of 80 min. The EIS measurements were performed under potentiostatic regulation at the corrosion potential (E_{corr}) in the frequency range [100 kHz ; 90 mHz] and by applying a 50 mV_{rms} amplitude perturbation. The detailed protocol has been previously described [8]. For the second step (Step 2 in Fig.1), the impedance spectra were recorded every 10 °C over the range [25 °C ; 75 °C]. The diagrams were collected at E_{corr} in the frequency range [100 kHz ; 10mHz] (10 points per decade) and by applying a 70 mV_{rms} amplitude perturbation. The amplitude perturbations were chosen in the linearity domain [20 mV_{rms} ; 100 mV_{rms}] as verified by a preliminary study. Due to the limitation of the corrosion process by the chemical conditioning of the solution, the applied amplitude perturbation can be increased in order to induce measurable OLDA dipole reactions to the applied field [12]. For the impedance analysis, data above 5 kHz were not considered due to experimental artefacts linked to the low conductivity (0.2 $mS.cm^{-1}$) of the electrolytic

solution [17].

3. Results and Discussion

I. Analysis of the "bulk" OLDA dielectric response

3.1. DSC analysis of OLDA

The DSC ramp (first heating) of "bulk" OLDA is reported in Fig. 2. The thermogram clearly shows that, from -25 °C to 35 °C, OLDA undergoes endothermic phase transitions which can be associated to a progressive transition from solid state to liquid state.

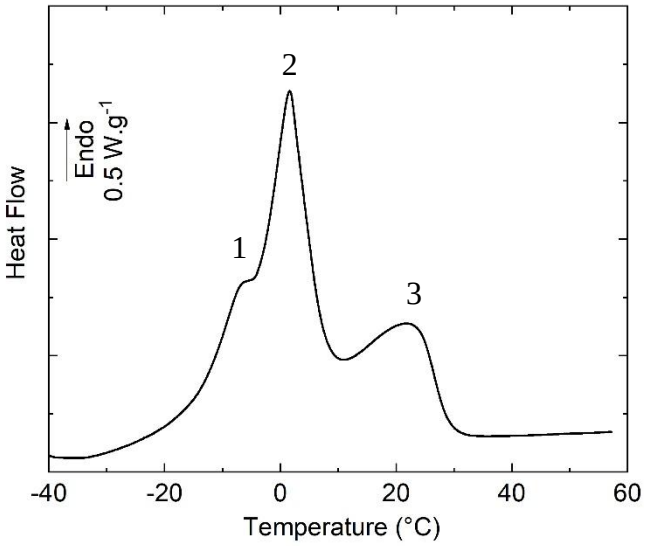

Fig. 2. DSC thermogram (heating ramp, 20 °C.min^{-1}) of OLDA.

The trimodal nature of the peak is difficult to interpret but it obviously reflects at least three (semi)crystalline phases which melt at different temperatures. At room temperature, OLDA presents, visually, at least two discernible phases, a liquid-like phase and a solid-like phase probably related to the first/second peaks and the third peak, respectively. Crystallization of organic molecules is described to be disturbed by the distribution of molecular conformations allowing a greater number of structural options available for crystallization and thus giving rise to polymorphs [18][19][20]. ^{1}H RMN analysis (data not

shown) indicated a *cis* configuration of the molecule (C=C double bond) which, in addition to possible molecular conformations, can participate to the polymorphism of OLDA. The 2 % impurities (ionic species and/or amines with shorter alkyl chains), can also contribute to the OLDA polymorphism, the study of which is out of scope for this paper. After 35 °C, the entirety of OLDA is found in the liquid-like state.

3.2. Analysis of the charge transport process in OLDA by BDS

The imaginary part, C'', of the complex capacitance related to dissipative phenomena inducing energy losses is presented as a function of temperature and frequency on the 3D relaxation map in Fig. 3.

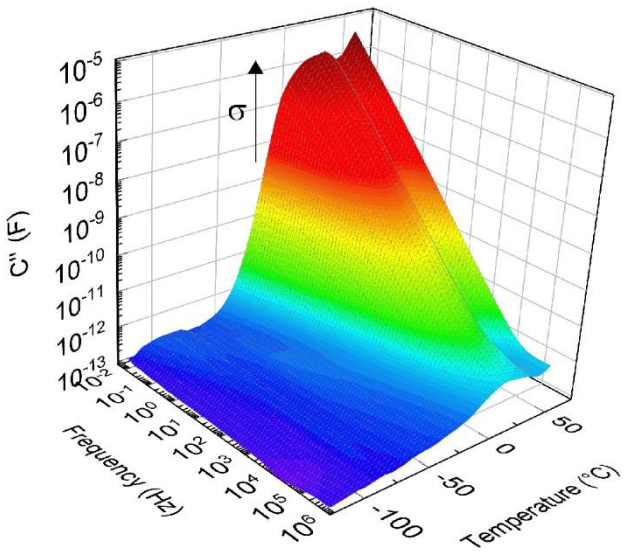

Fig. 3. 3D dielectric relaxation maps of "bulk" OLDA as obtained from BDS measurements.

For low temperatures ranging from -110 °C to -50 °C, two peaks in C"(ω) characteristics of relaxation modes of organic (macro)molecules can be observed. At low frequency and for a temperature range [-20 °C ; 50°C], a conductivity rise becomes dominant. Complementary experiments conducted on the interdigitated electrode without any deposited OLDA showed that for temperatures from -150 °C to -20 °C, the obtained signal in Fig. 3 contained contributions from both the electrode substrate and the OLDA molecules. If OLDA

presents any molecular mobility modes, based on SAM literature, they are likely to manifest at this temperature range [11][21]. However, no molecular mobility mode could be identified for OLDA "bulk", probably due to a weak dipolar response compared to the interdigitated electrode substrate. From -20 °C to 50 °C, at low frequency, an increase of about three decades of the complex capacity in the presence of OLDA was noted. The phenomena that occur at low frequency and high temperature can therefore be attributed to the OLDA and can be related to the charge transport (conductivity) in the sample and/or to the charge accumulation at the electrode interfaces [9]. Furthermore, an isotherm mode can be clearly distinguished at 40 °C in Fig. 3.

The experimental data were converted to the electrical conductivity $\sigma^*(\omega)$ formalism according to Eq. 4, to emphasize the charge transport processes. The real part ($\sigma'(\omega)$) of the complex conductivity, related to the dissipative part of $C^*(\omega)$ is showed in Fig. 4 as a function of frequency and temperature. For temperatures from -25 °C to 30 °C (Fig. 4a), the conductivity spectra present low frequency *dc* conductivity plateaus, where the conductivity is independent of frequency, and high frequency power-law describing the resistive and capacitive behaviour of the analysed sample, respectively. The spectra seem to obey to the "universal dielectric relaxation response" of disordered (non-crystalline) materials as stated by Jonscher [22]. The low frequency domain reflects the charge transport processes whose mechanisms are thought to be thermally assisted hopping of charge carriers (electrons and/or ions) *via* localized states which lead to macroscopic conductivity over the analysed sample [23][24][10]. On the other hand, the high frequency power law reflects the inability of charge carriers to follow the applied field. From -5 °C, a significant decrease in conductivity can be observed at low frequency, beyond the *dc* conductivity plateaus, which can be related to electrode polarization phenomena and can result from the accumulation of charges on electrode interfaces [9]. From 35 °C (Fig. 4b), these phenomena became less pronounced.

Furthermore, for temperatures from 35 °C to 50 °C, a slight conductivity step can be observed between 10^5 and 10^3 Hz corresponding to the transition from the high frequency power law to the low frequency *dc* conductivity plateaus. The conductivity steps, in polymer domain, are associated to specific modes of molecular mobility of the polymer such as α-mode (dielectric manifestation of the glass transition). However, no glass transition was identified for OLDA at the investigated temperature range (DSC measurements in Fig. 2).

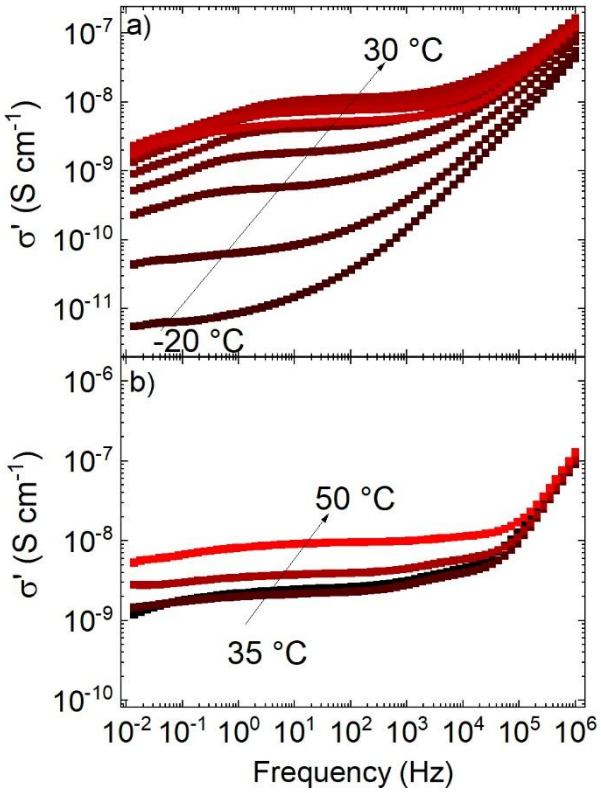

Fig. 4. Real part of the electrical conductivity calculated from BDS complex impedance measurements on OLDA "bulk" a) from -25 °C to 30 °C and b) from 35 °C to 50 °C. The temperature step between each spectrum is 5 °C.

The *dc* conductivities were extracted from the frequency independent plateaus and are reported on an Arrhenius diagram (Fig. 5). Three domains can be distinguished. First, in domain I (from -25 °C to 10 °C) an increase of nearly two decades of the *dc* conductivity values can be observed. Then, from 10 °C to 40 °C (domain II), the *dc* conductivity values decrease from 1.10^{-8} to 2.10^{-9} S.cm^{-1}. This temperature range corresponds to the progressive

transition of OLDA from a solid-like state to a liquid-like state as observed in DSC measurements. The increase in the conductivity can therefore be attributed to the progressive transformation of organized solid-like structure of OLDA (probably with different (semi)crystalline phases) into a looser organization of the molecules in the liquid-like state. In domain III (from 40 °C to 50 °C), the *dc* conductivity values increase with temperature corresponding to the liquid-like state of OLDA. The 40 °C temperature corresponds to the isotherm mode noted on the 3D relaxation map (Fig. 3) and to the temperature at which OLDA is entirely in the liquid-like state (DSC measurements).

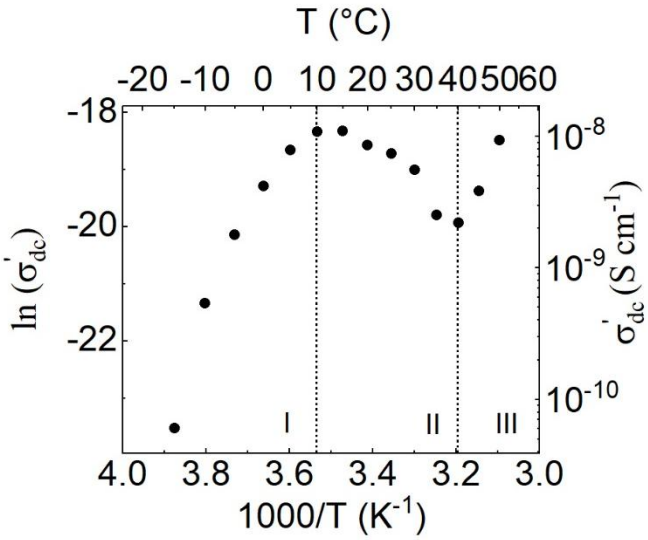

Fig. 5. Arrhenius plots of the *dc* conductivity determined from BDS measurements of OLDA.

To summarize, no dipolar relaxation modes were identified at low temperature. BDS analyses highlighted the thermal activation of "bulk" OLDA conductivity in the solid-like state at low temperatures and in the liquid-like state at temperatures above 35 °C. The latter is described by a resistive behavior over a wide frequency domain [10^{-2} Hz ; 10^{4} Hz] and a capacitive behavior only for frequencies higher than 10^{4} Hz. The conductivity is strongly influenced by solid-like to liquid-like transition as observed in DSC analyses.

II. Analysis of the adsorbed OLDA layer onto the steel surface

By analogy to the BDS methodology for the study of "bulk" OLDA, the adsorbed OLDA layer onto the steel surface will be analysed as a function of temperature. First, *ex situ* PM-IRRAS analysis were conducted to investigate the OLDA layer thickness and the molecular structure in the temperature range [25 °C ; 75 °C]. Then, for the same temperature range, the OLDA response in EIS spectra is analyzed.

3.3. Ex situ surface characterization by PM-IRRAS

The OLDA layer was formed during 80 min in a deaerated solution at a $pH_{25°C}$ = 11 for three different temperatures, 25 °C, 50 °C and 75 °C and the IRRAS spectra are shown in Fig. 6.

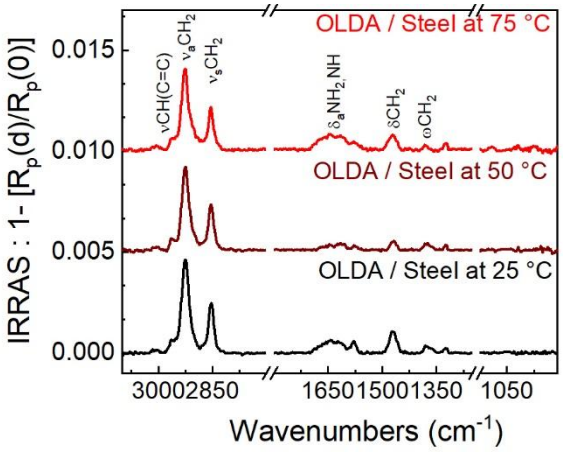

Fig. 6. *Ex situ* IRRAS spectra of the OLDA layer adsorbed onto the carbon steel surface after 80 min of immersion in a deaerated solution containing 100 $mg.kg^{-1}$ of OLDA at a $pH_{25°C}$ = 11 for three temperatures 25 °C, 50 °C and 75 °C.

The three IRRAS spectra showed bands at 3004, 2925, 2854, 1470 and 1375 cm^{-1} attributed to the stretching CH mode of the unsaturated C=C bonds (νCH(C=C)), to the asymmetric (ν_aCH_2) and symmetric (ν_sCH_2) stretching modes of methylene groups, to the bending mode of methylene groups (δCH_2) and to the wagging modes of the methylene groups (ωCH_2), respectively. Furthermore, in the 1700-1500 cm^{-1} range, two main

contributions can be observed at 1650 and 1578 cm^{-1}. Apart from the bending modes of the NH_2 and NH groups, other species are probably formed at the steel surface such as the -NH-COO^- group, as previously reported [8][25]. Finally, no band relative to corrosion products (iron oxides or hydroxides) is observed on the IRRAS spectra for all the studied temperatures, confirmed by visual inspections of the carbon steel surface as well. However, the presence of a nanometric thin oxide layer formed for these experimental conditions [26][27] and not detectable by PM-IRRAS cannot be excluded.

The IRRAS intensity of the $\nu_a CH_2$ can be used to estimate the OLDA layer thickness onto carbon steel, as previously reported [8]. The estimated thicknesses are 1.8 nm at 25 °C, 1.6 nm at 50 °C and 1.5 nm at 75° C. It is important to note that the provided thicknesses (only meaningful for isotropic and compact arrangement of OLDA molecules onto carbon steel surface) should not be considered for their absolute values but more as an order of magnitude of the adsorbed OLDA molecules. It seems that, for these experimental conditions where the corrosion processes are very limited (absence of infrared bands of lepidocrocite γ-FeOOH at 1020 cm^{-1}) and the initial OLDA concentration in the solution is relatively high (100 $mg.kg^{-1}$), the estimated thickness values correspond to an OLDA monolayer formed onto the steel surface independently of the temperature over the range [25 °C ; 75 °C]. The values are similar to those determined for OLDA adsorbed on model surfaces such as mica [25][28] or those determined for OLDA adsorbed on gold [8]. It confirms thusly the role of corrosion products on the OLDA accumulation onto the carbon steel surface (thicknesses greater than the monolayer) and the formation of mixed layers OLDA/corrosion products as discussed in our previous work [8]. The wavenumbers of $\nu_a CH_2$ and $\nu_s CH_2$ bands at 2925 and 2854 cm^{-1}, respectively, indicate *gauche* defects in the alkyl chains [29] due to the *cis* configuration of the molecule. The presence of *gauche* defects can promote a disordered layer in agreement with previous studies [8][30].

In the next section, the dielectric response of "bulk" OLDA and the molecular structure of the adsorbed OLDA layer will be used as "references" to analyse the OLDA response in the EIS diagrams of the electrochemical system steel/OLDA/electrolyte.

3.4. OLDA adsorption kinetics monitored by EIS at 25 °C

First, the OLDA layer was formed onto the carbon steel surface at 25 °C. Its adsorption kinetics was monitored by EIS. Fig. 7 shows some impedance spectra [5 kHz ; 90 mHz] recorded for immersion times from 2 min to 80 min at 25 °C. The complete spectra [5 kHz ; 10 mHz] corresponding to an immersion time of 100 min is also reported in Fig. 7.

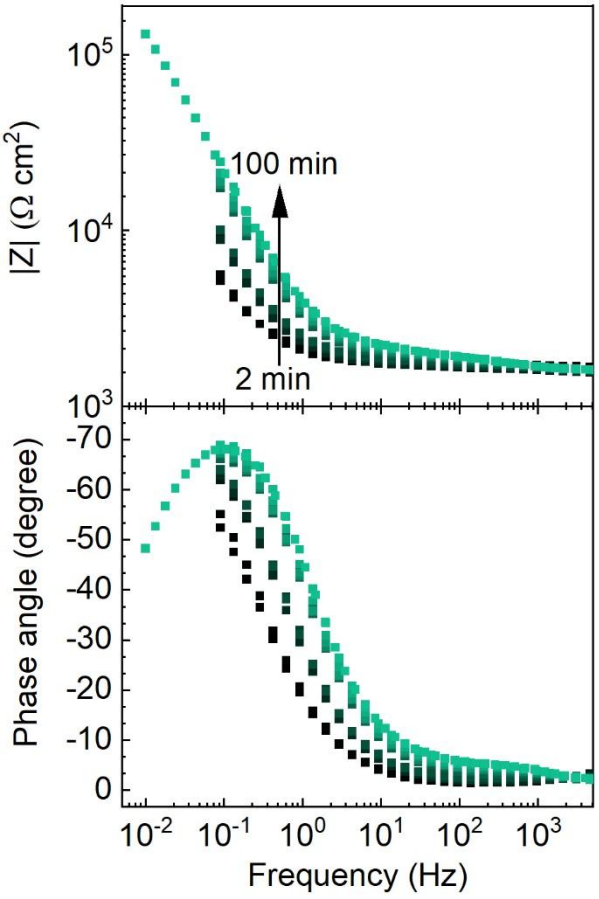

Fig. 7. EIS diagrams (Bode plots non-corrected from R_e) *vs*. immersion time from 2 min to 100 min for the carbon steel immersed in a deaerated solution containing 100 mg.kg^{-1} of OLDA, $pH_{25°C}$ = 11 at 25 °C.

The diagrams exhibit predominantly a time constant at low frequency [10 Hz ; 10 mHz] associated to the electrolyte/metal interface phenomena and characterized by a charge

transfer resistance (R_{tc}) and a double layer capacitance (C_{dl}). In the high frequency domain [5 kHz ; 10 Hz], a second time constant can be guessed associated to the presence of OLDA onto the carbon steel surface according to the literature [2][7][8].

Regarding the adsorption kinetics, the impedance modulus and the phase angle in the low frequency domain increase progressively over immersion time. The time constant in the high frequency domain is formed over immersion time as indicated from the slight impedance modulus and phase angle increase in this frequency domain. The impedance data suggest the progressive adsorption of OLDA onto the carbon steel surface without the simultaneous formation of corrosion products, as compared to our previous work [8] and confirmed by the PM-IRRAS analyses (Fig. 6).

Impedance diagrams (Bode plots) are powerful in revealing the resistive contributions from the electrochemical interface such as faradaic reactions and diffusion-controlled reactions. However, it has been shown recently that this formalism is not optimal for the study of dielectric signature of organic layers, such as polymers [12] and SAM/gold surfaces [31][32]. The complex capacitance formalism, on the other hand, allows the capacitive contributions of a dielectric system to be highlighted. The features of the complex capacitance would be related to dipole relaxation processes. C'(ω) is associated with energy storage (conservative phenomena) whereas C"(ω) to energy losses (dissipative phenomena) due to electrical charge transport or molecular mobility modes. Bueno *et al*. [31] have adopted these formalism to explain the dielectric response of SAM layers adsorbed onto gold surfaces. The adsorption of organic molecules onto a metallic surface would first cause a decrease of the electrochemical double layer capacitance and, in addition, SAM dipolar relaxation processes.

The impedance diagrams were, therefore, transformed in complex capacitance by means of Eq. 4. The real part (C'(ω)) and imaginary part (C"(ω)) of the complex capacitance corrected from the electrolyte resistance (R_e) are showed in Fig. 8a and Fig. 8b, respectively.

R_e of a value of approximately 1600 Ω.cm^2 was considered constant during the adsorption process and it was determined from the real part of the impedance modulus at 5 kHz.

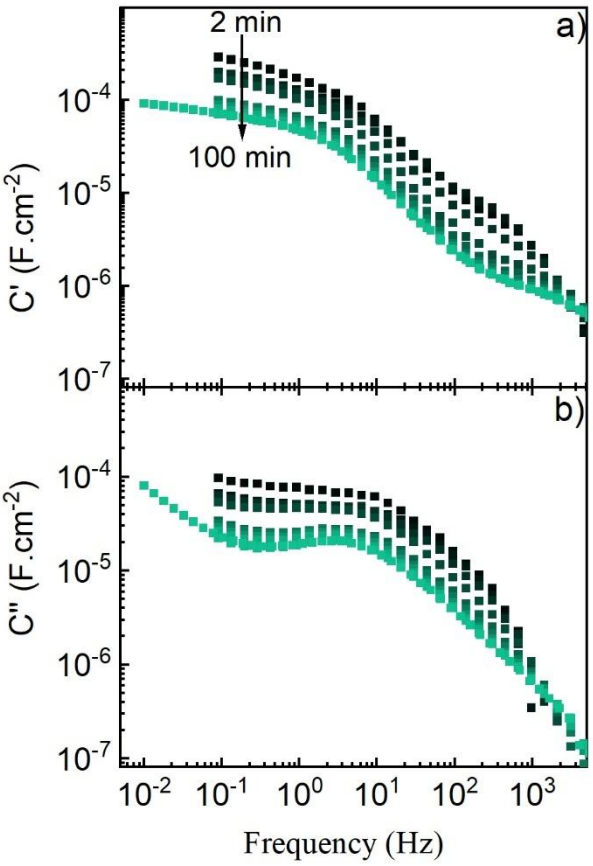

Fig. 8. Complex capacitance spectra corrected from R_ea) real part (C') and b) imaginary part (C'') obtained from the EIS measurements during the monitoring of the OLDA adsorption kinetics from 2 min to 100 min.

A decrease of the real and imaginary capacitance values is noted in Fig. 8. Water molecules, as well as other ionic species, initially present in the solution and onto the carbon steel surface are progressively replaced by the OLDA molecules during the adsorption process. The capacitance variations over immersion time could reflect modifications of the electrochemical double layer capacitance due to the OLDA adsorption [33][34][35][36] over all the studied frequency range. With regard to the complex capacitance spectra features: a step-like decrease of the real part C'(ω) with increasing frequency and a peak in the imaginary part C''(ω) appear when the immersion time increases and can be clearly seen after 100 min of

immersion. The real capacitance plateau at low frequency could be related to the pseudo-capacitance describing the electrochemical double layer as it will be discussed further in the paper. At high frequency, the plateau would be related to a modified interfacial capacitance due to the OLDA adsorption. The capacitance step would reflect the resistive behavior of the OLDA layer as previously observed in BDS measurements. This hypothesis is supported by the Bode plots (Fig. 7) which show two time constants. The C"(ω) peak would be more likely attributed to a mathematical convolution of the two time constants and not to a relaxation process (Debye type relaxation) due to field-free reorientational and translational motions of OLDA dipoles as reported for SAM layers [31]. Finally, the increase of the C"(ω) at low frequency range [10^{-1} Hz ; 10^{-2} Hz] may indicate a contribution of charge transport of ionic species onto the steel surface as a parallel to polymer systems [11].

To further support and elaborate on these hypotheses, the following section aims to analyze the temperature dependence of the response of the electrochemical system in order to dissociate contributions originating from the OLDA layer and the electrochemical double layer.

3.5. Temperature dependence of OLDA conductivity and of the electrochemical double layer capacitance in EIS experiments

3.5.1. EIS diagrams as a function of temperature

Impedance diagrams recorded for the adsorbed OLDA onto the carbon steel surface from 25 °C to 75 °C, non-corrected and corrected from the electrolyte resistance (R_e) are shown in Fig. 9a and Fig. 9b, respectively. In this part, the eventual desorption of OLDA molecules with temperature rise can be ruled out based on the PM-IRRAS analyses as previously discussed.

For non-corrected diagrams, the impedance modulus in the high frequency domain corresponds to the electrolyte resistance (R_e). R_e decreases from 2000 Ω.cm^2 to approximately

500 Ω.cm^2 with temperature increase due to the increase of the solution conductivity, R_e being proportional to the inverse of the solution conductivity [37]. In the medium frequency domain [1 Hz ; 10^{-1} Hz], the impedance modulus features a quasi-linear rise with frequency decrease and the EIS spectra are superimposed for all the studied temperatures. In the low frequency domain [10^{-1} Hz ; 10^{-2} Hz], the impedance modulus decreases with temperature increase.

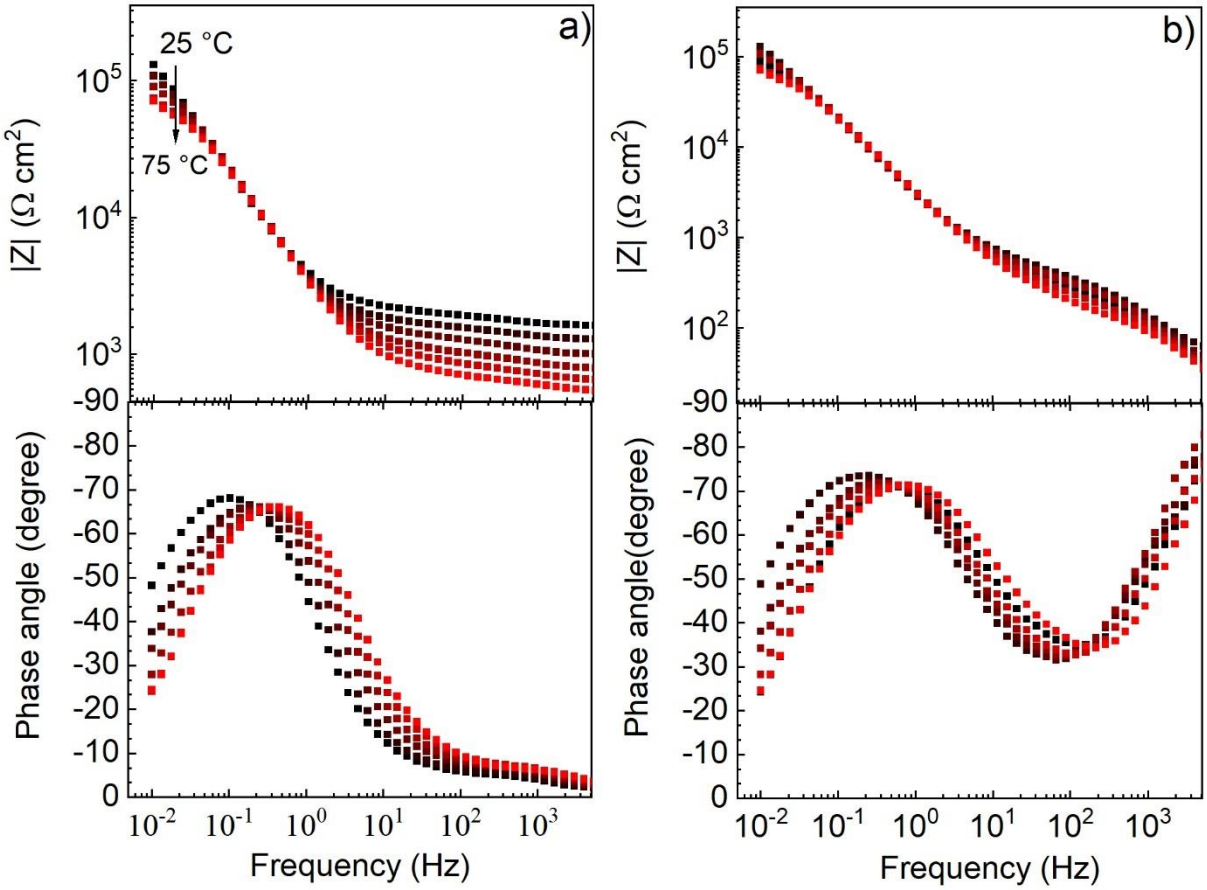

Fig. 9. EIS diagrams (Bode plots) a) non-corrected and b) corrected from the electrolyte resistance (R_e) obtained for the OLDA / steel system for different temperatures. The temperature step between each diagram is 10 °C.

It has been demonstrated that the R_e contribution masks the capacitive response at high frequency [2][38] and influences the extracted parameters. The EIS spectra for each temperature were therefore, corrected from R_e and the corresponding values are presented in Table. 2. The R_e correction reveals a shoulder on the impedance modulus between 5 kHz and 10 Hz, revealing a resistive behavior of the system. Regarding the phase angle, a plateau

corresponding to a CPE behavior as previously reported for ODA layers [2] is not highlighted in the exploitable frequency domain.

3.5.2. Analysis of the high frequency time constant: complex capacitance and conductivity formalisms

The complex capacitance formalism (Fig. 10) was applied to investigate the temperature influence on the dielectric signature of the adsorbed OLDA layer onto the carbon steel surface.

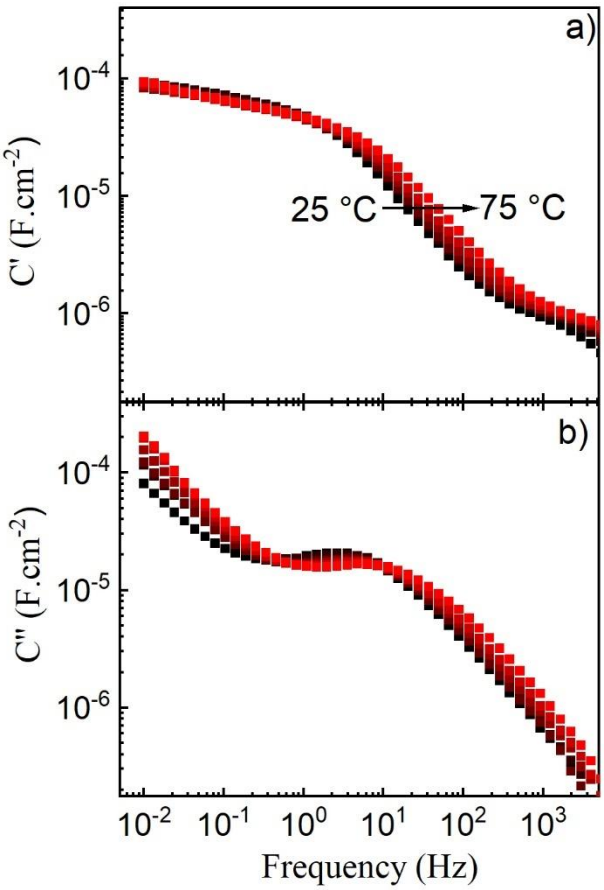

Fig. 10. Complex capacitance spectra a) real part (C') and b) imaginary part (C'') obtained from the EIS measurements for different temperatures from 25 °C to 75 °C.

The same spectral features are observed as before (Fig.8). The C'(ω) plateaus at low frequency does not vary with temperature. From 10^2 Hz to 1 Hz, C'(ω) shifts to higher frequencies with temperature increase. From 5 kHz to 10^2 Hz, C'(ω) increases with temperature rise. C''(ω) shifts to higher frequencies with temperature rise over all the

frequency range and at the low frequency range it increases with temperature.

In order to draw a comparison with the BDS results, the impedance data of the electrochemical system steel/OLDA/solution were transformed into the complex conductivity formalism according to Eq. 5. Two assumptions were made to transform the impedance data into complex conductivity; a total coverage of the steel surface (A = 1 cm^2) and the OLDA layer thickness was taken as 1.6 nm independently of the temperature as estimated by *ex situ* PM-IRRAS analyses. However, these assumptions are crude because the coverage of surface is not total as it will be discussed further and the thickness of the layer can be slightly higher *in situ*.

The real part of the conductivity σ'(ω) as a function of frequency and temperature is reported in Fig. 11.

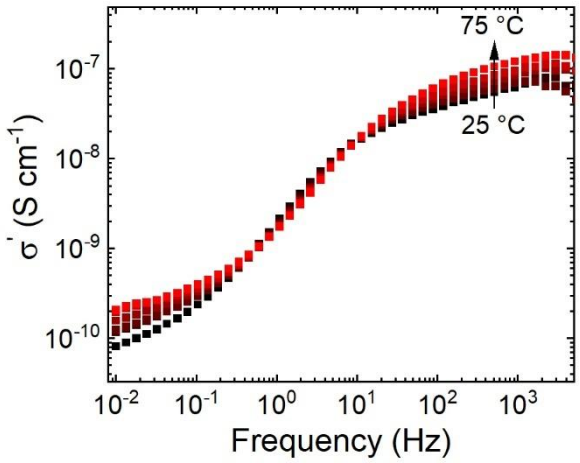

Fig. 11. Real part of the electrical conductivity (σ' (ω)) calculated from the EIS spectra performed on the adsorbed OLDA layer during temperature variations.

The conductivity spectra exhibit pseudo-conduction plateaus from 5 kHz to 10^2 Hz, a frequency range assumed to be associated with OLDA, but a power-law behaviour at higher frequencies is not observed as for the "bulk" OLDA spectra in the BDS measurements or as seen in EIS for immersed polymer systems [10]. The pseudo-conduction plateaus are followed by a quasi-linear decrease of the conductivity with frequency decrease corresponding to the frequency range in the Bode plots where the impedance modulus is also quasi-linear. The low

frequency range presents pseudo-conduction plateaus as well, probably due to charge transport of ionic species onto the steel surface, but due to the made assumptions which pertain only to an ideal layer of OLDA, this frequency range will not be discussed further.

The capacitance values at 1 kHz (high frequency pseudo-plateaus) and the conductivity values at 300 Hz (on the pseudo-conduction plateaus) were extracted and reported in an Arrhenius diagram (Fig. 12).

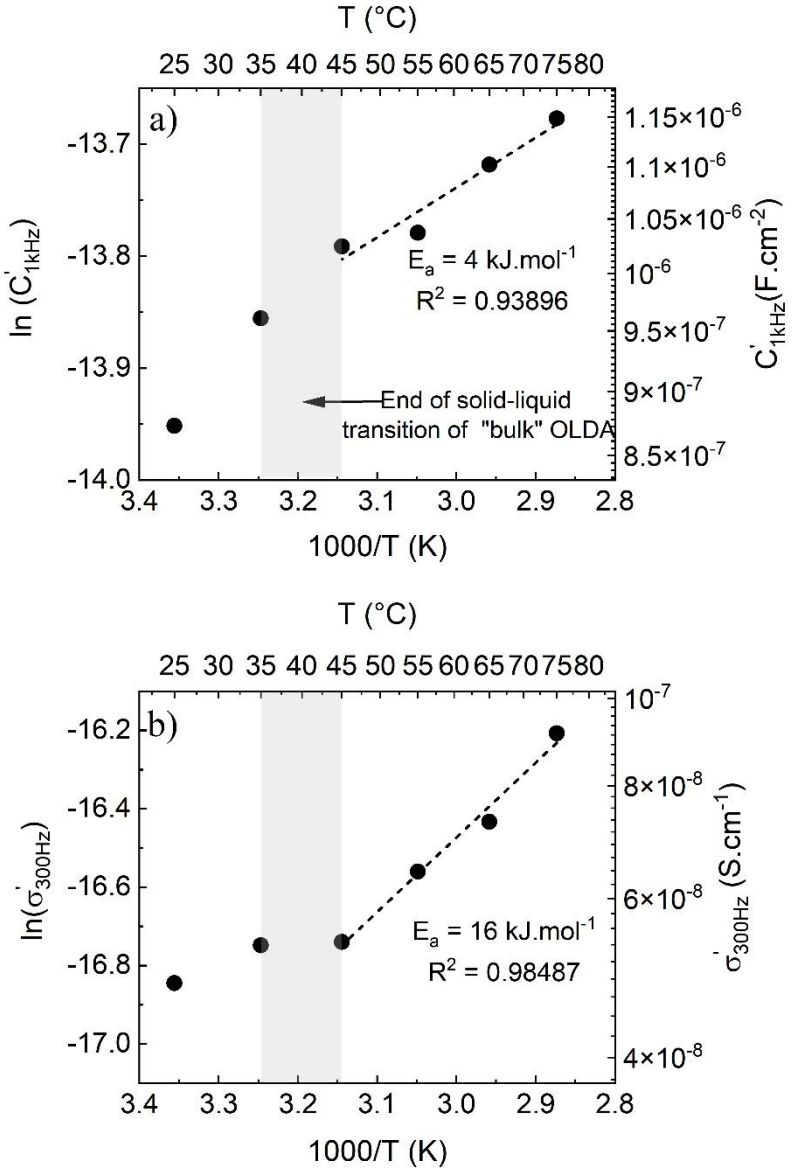

Fig. 12. Arrhenius diagram of the a) real capacitance extracted at 1 kHz (Fig. 10a) and b) real conductivity extracted at 300 Hz (Fig. 11) from the EIS measurements for the different temperatures.

The real capacitance values increase from $8.5.10^{-7}$ to $1.1.10^{-6}$ F.cm^{-2} with temperature increase with a subtle change in slope around 45 °C. The conductivity value can be considered as constant and from 45 °C to 75 °C, a linear increase is noted as temperature increases, corresponding to an Arrhenius dependence. The change in slope of the conductivity occurs between 35 and 45 °C which corresponds approximately to the end of solid-like to liquid-like phase transition of OLDA "bulk". It could be possible that with the increase in temperature, an alkyl chain "melting" transition of the OLDA molecules occurs on the steel surface. The same phenomenon has been described by Badia *et al*. [39] for melting transitions of alkanethiolate monolayers self-assembled on Au nanoparticles. Before the melting point, the alkyl chains are ordered in crystalline-like or gel-like state due to chain-chain Van der Waals interactions. Beyond the melting point, a disordered state has been noted, associated to the increase of the conformational *gauche* defects in the alkyl chains [40][41][42]. At 25 °C, the OLDA layer is already disordered on the surface due to the *cis* configuration of the molecule as previously discussed. As the number of *gauche* defects increases with temperature, the chain free volume should increase as proposed by Badia *et al*. [39] as well as the chains mobility and in consequence the OLDA layer disorder should increase. PM-IRRAS analyses did not reveal an increase in the *gauche* defects number with temperature. It is possible that the phase transition is reversible and as the analyses are carried out at room temperature, the additional conformational *gauche* defects are not detected.

The activation energy (E_a) for the OLDA layer conductivity and the capacitance were calculated according to Eq. 6 for the temperature range [45 °C ; 75 °C]. These values were 16 kJ.mol^{-1} (0.16 eV) and 4 kJ.mol^{-1} (0.04 eV), respectively. The capacitance activation energy could suggest the formation of *gauche* defects. The reported values in literature are on the order of 0.022 eV [41]. The conductivity activation energy will be compared in the next sections with the activation energy of the low frequency phenomena.

$$\sigma = \sigma_0 \exp(-\frac{E_a}{RT}) \quad \textbf{(6)}$$

Where σ_0 is the pre-exponential factor ($S.cm^{-1}$), E_a the activation energy ($kJ.mol^{-1}$), R the ideal gas constant (8.314 $J.K^{-1}.mol^{-1}$) and T the temperature (K).

3.5.3. Analysis of the time constant at low frequency

A classical approach was applied to investigate the impedance variations in the low frequency domain with temperature increase. The CPE parameters (Q_{dl}, α_{dl}), the charge transfer resistance (R_{ct}) of the low frequency time constant, and the electrolyte resistance (R_e) at high frequency were determined. The Q_{dl}, α_{dl} and R_e were graphically assessed by using a graphical method [43] and by extrapolation of the real part of the impedance modulus in the high frequency domain, respectively. The R_{ct} values, however, cannot be accurately determined because the impedance modulus in the low frequency region does not reach a resistive plateau (phase angle is different from zero). Thus, the low frequency time constant for each temperature was fitted with a simple R//CPE electrical equivalent circuit (EEC). The Q_{dl}, α_{dl}, R_{ct} and R_e values graphically determined and from the EEC are reported in Table. 2. It can be seen from Table 2, that the Q_{dl} and α_{dl} values do not vary with the temperature and the two methods lead to comparable results. The Q_{dl} and α_{dl} were determined in the frequency range where the impedance modulus (Fig. 9) and the conductivity (Fig. 11) are quasi-linear with temperature increase. Furthermore, the estimated values correspond to the capacitance plateau values at low frequency (Fig. 10a) (64 $\mu F.cm^{-2}$). This supports the hypothesis that the capacitance plateau at low frequency is related to the electrochemical double layer capacitance. On the contrary, the R_{ct} and R_e values decrease with temperature increase with an Arrhenius behavior, in the whole temperature range, reflecting the observed variations from the impedance spectra (Fig. 9). The activation energy calculated from both these parameters was approximately 20 $kJ.mol^{-1}$. This could suggest that the thermal

activation of charge transfer mechanisms occurring at the carbon steel/electrolyte interface is governed by the ion mobility (electrolyte resistance). The calculated activation energy values are comparable to that obtained from the OLDA conductivity variation (16 kJ.mol^{-1}) in the temperature range [45 °C ; 75 °C].

Table 2

R_e, Q_{dl}, α_{dl}, R_{ct} values as a function of temperature estimated graphically and from the adjustment of the low frequency time constant with an R // CPE electrical equivalent circuit.

T (°C)	R_e **(Ω.cm^2)**		Q_{dl} **(μF.cm^{-2}s$^{(\alpha-1)}$)**		α_{dl}		R_{ct}**(kΩ.cm^2)**
	Graphical estimation	EEC adjustment	Graphical estimation	EEC adjustment	Graphical estimation	EEC adjustment	EEC adjustment
25	1600	2098	71	69	0.85	0.86	311
35	1275	1699	73	71	0.82	0.85	197
45	995	1334	68	64	0.82	0.84	176
55	780	991	70	63	0.81	0.83	132
65	640	722	70	62	0.80	0.81	98
75	530	593	73	64	0.78	0.82	90

The *gauche* defects of the alkyl chains are favorable to the presence of structural defects that allow the electrolyte to reach the interface (PM-IRRAS analyses). The possible "melting" of the alkyl chains between 35 °C and 45 °C (DSC and BDS analyses) could promote the increase of the conformational *gauche* defects [41] and increase the disorder in the layer. The ions and water traverse the OLDA layer through the defects and/or the free volume which would explain the same temperature dependence of the phenomena manifested at high and low frequency [44].

Considering the coexistence of OLDA molecules and solution ions at the interface, it is likely that the high frequency capacitance response previously discussed, reflects the

capacity of OLDA, but also contains contributions of the double layer [45]. The pseudo-plateau at high frequency on the capacitance spectra (Fig. 8 and Fig. 10) could be thusly related to a modified double layer capacitance due to the OLDA adsorption. It is therefore difficult to consider a representation of the system in which the surface of the metal would be, in places, bare (pore-like) and that elsewhere the OLDA would form a monolayer film presenting the capacity of the OLDA. Instead, the capacitive response of the interface appears to be the sum of the response of the double layer on the unprotected surface (incomplete surface coverage) (C_{dl}) and the response of the double layer modified by the adsorption of OLDA molecules (modified C_{dl}). A schematic representation of the interface for these experimental conditions is given in Fig. 13. Given the multitude of capacitive contributions in the high frequency domain and in consequence the non-total surface coverage, the determination of the OLDA layer thickness through the model of an ideal Helmholtz capacitor does not appear appropriate.

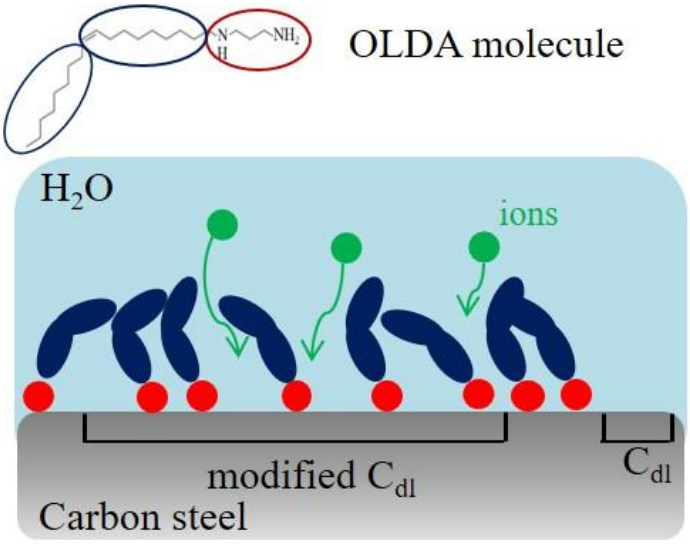

Fig. 13. Schematic representation of the interface.

4. Conclusions

A film-forming amine, N-oleyl propanediamine (OLDA), commonly used for the protection of carbon steel surfaces against corrosion, was analysed in the present work with the aim to investigate its dielectric contribution on impedance spectra. First, the OLDA "bulk" was studied by BDS. Even though no dipolar relaxation was identified at low temperature, the thermal activation of the OLDA conductivity was highlighted. The conductivity was shown to strongly depend on solid-liquid transition of the OLDA molecules, as confirmed by DSC analyses. Thusly, the conductivity manifested in a large range of temperature, from -25 °C to 35 °C in the OLDA solid-like state and above 35 °C in the liquid-like state. The impedance spectra seemed to obey to the "universal dielectric relaxation response" (Jonscher law). In the liquid-like state, a resistive behaviour over a wide frequency domain [10^{-2} Hz ; 10^{4} Hz] and a capacitive behaviour only for frequencies higher that 10^{-4} Hz were emphasised by the complex conductivity formalism.

In order to analyse the adsorbed OLDA layer onto a carbon steel surface response in electrochemical impedance spectra, the same methodology as before was applied. EIS measurements were performed at constant temperature in the range [25 °C ; 75 °C] and the complex capacitance and conductivity formalisms were applied to the impedance data. The capacitance formalism allowed to highlight the capacitive behaviour at low frequency, associated to the electrochemical double layer, and at high frequency, associated to a modified electrochemical double layer by the OLDA adsorption onto the steel surface. No dipolar relaxation modes were identified in this temperature range. The conductivity formalism allowed to emphasize the OLDA resistive behaviour. By analysing the temperature dependency of the high frequency capacitance, the formation of conformational *gauche* defects on the OLDA alkyl chain was noted for temperatures higher that 45 °C, possibly corresponding to a chain "melting" phenomenon. The conformational *gauche* defects on the

OLDA alkyl chain in addition to the configurational ones, the latter confirmed by ^{1}H NMR and *ex situ* PM-IRRAS analyses would increase the disorder in the OLDA layer and in consequence the chain free volume. This could promote the infiltration of ions and water through the free volume of layer. The hypothesis is supported from the same temperature dependency of the OLDA conductivity and the electrolyte resistance. Finally, the ion mobility seemed to also govern the charge transfer mechanisms occurring at the carbon steel/electrolyte interface.

This methodology could be considered to further analyse and interpret the response in impedance spectra by applying to other small organic molecules with different chemistry. It can also be used to further investigate the effects of structural confinement of organic layers by increasing or decreasing the ordering of the layer in both dry (bulk or adsorbed) and immersed state.

CRediT authorship contribution statement

Deni Jero: Conceptualization, Data curation, Formal analysis, Investigation, Methodology, Writing - original draft. **Nicolas Caussé:** Conceptualization, Formal analysis, Investigation, Methodology, Project administration, Supervision, Validation, Writing - review & editing. **Eric Dantras:** Investigation, Writing - review & editing. **Aurélien Roggero:** Investigation, Writing - review & editing. **Thierry Buffeteau:** Investigation, Writing - review & editing. **Nadine Pébère:** Conceptualization, Formal analysis, Investigation, Methodology, Project administration, Supervision, Validation, Writing - review & editing.

Data availability

The raw/processed data required to reproduce these findings cannot be shared at this time as the data also forms part of an ongoing study.

Acknowledgments

This work was carried out with the financial support ODYSSEE Environnement. The authors gratefully acknowledge the partners of the project: Fabrice Chaussec and Amaury Buvignier of ODYSSEE Environnement as well as Marion Roy of CEA Saclay.

Declaration of competing interest

The authors declare that they have no known competing financial interests or personal relationships that could have appeared to influence the work reported in this paper.

References

[1] I. Betova, M. Bojinov, T. Saario, Film-forming amines in steam / water cycles – structure, properties, and influence on corrosion, Tech. Res. Cent. Finl., VTT-R-0323 (2014) 1–41.

[2] J. Baux, N. Caussé, S. Delaunay, J. Tireau, M. Roy, D. You, N. Pébère, Impedance analysis of film-forming amines for the corrosion protection of a carbon steel, Electrochim. Acta, 283 (2018) 699–707, doi: 10.1016/j.electacta.2018.06.189.

[3] P. Bommersbach, C. Alemany-Dumont, J. P. Millet, B. Normand, Formation and

behaviour study of an environment-friendly corrosion inhibitor by electrochemical methods, Electrochim. Acta, 51 (2005) 1076–1084, doi: 10.1016/j.electacta.2005.06.001.

[4] W. Kuang, J. A. Mathews, M. L. Taylor, D. D. Macdonald, The effect of Anodamine on the corrosion behavior of 1018 mild steel in deionized water: II. Electrochemical Impedance Analysis, Electrochim. Acta, 136 (2014) 493–503, doi: 10.1016/j.electacta.2014.05.146.

[5] M. P. Desimone, G. Gordillo, S. N. Simison, The effect of temperature and concentration on the corrosion inhibition mechanism of an amphiphilic amido-amine in CO_2 saturated solution, Corros. Sci., 53 (2011) 4033–4043, doi: 10.1016/j.corsci.2011.08.009.

[6] M. P. Desimone, G. Grundmeier, G. Gordillo, S. N. Simison, Amphiphilic amido-amine as an effective corrosion inhibitor for mild steel exposed to CO_2 saturated solution: Polarization, EIS and PM-IRRAS studies, Electrochim. Acta, 56 (2011) 2990–2998, doi: 10.1016/J.ELECTACTA.2011.01.009.

[7] J. Baux, N. Caussé, S. Delaunay, J. Tireau, M. Roy, D. You, N. Pébère, Film-forming amines for the corrosion protection of carbon steels in nuclear power plant secondary circuit conditions: an impedance study, J. Electrochem. Soc., 167 (2020) 061504, doi: 10.1149/1945-7111/ab7d42.

[8] D. Jero, N. Caussé, O. Marsan, T. Buffeteau, F. Chaussec, A. Buvignier, M. Roy, N. Pébère, Film-forming amines adsorption and corrosion kinetics on carbon steel surface in neutral solution investigated by EIS and PM-IRRAS analysis, Electrochim. Acta, 443 (2023) 141925, doi: 10.1016/J.ELECTACTA.2023.141925.

[9] F. Kremer, A. Schönhals, Broadband dielectric spectroscopy, Springer, (2003).

[10] A. Roggero, N. Caussé, E. Dantras, L. Villareal, A. Santos, N. Pébère, Thermal activation of impedance measurements on an epoxy coating for the corrosion protection: 1. Dielectric spectroscopy response in the dry state, Electrochim. Acta, 303 (2019) 239–245, doi: 10.1016/j.electacta.2019.02.035.

[11] M. C. Scott, D. R. Stevens, J. R. Bochinski, L. I. Clarke, Dynamics within alkylsiloxane self-assembled monolayers studied by sensitive dielectric spectroscopy, ACS Nano, 2 (2008) 2392–2400, doi: 10.1021/nn800543j.

[12] A. Roggero, N. Caussé, E. Dantras, L. Villareal, A. Santos, N. Pébère, Thermal activation of impedance measurements on an epoxy coating for the corrosion

protection: 2. electrochemical impedance spectroscopy study, Electrochim. Acta, 305 (2019) 116–124, doi: 10.1016/j.electacta.2019.03.007.

[13] T. Buffeteau, B. Desbat, J. M. Turlet, Polarization modulation FT-IR spectroscopy of surfaces and ultra-thin films: experimental procedure and quantitative analysis, Appl. Spectrosc., 45 (1991) 380–389, doi: 10.1366/0003702914337308.

[14] T. Buffeteau, B. Desbat, D. Blaudez, J. M. Turlet, Calibration procedure to derive IRRAS spectra from PM-IRRAS spectra, Appl. Spectrosc., 54 (2000) 1646–1650, doi: 10.1366/0003702001948673.

[15] M. A. Ramin, G. Le Bourdon, N. Daugey, B. Bennetau, L. Vellutini, T. Buffeteau, PM-IRRAS investigation of self-assembled monolayers grafted onto SiO_2/Au substrates, Langmuir, 27 (2011) 6076–6084, doi: 10.1021/la2006293.

[16] E. Jäppinen, T. Ikäläinen, F. Lindfors, T. Saario, K. Sipiläa, I. Betova, M. Bojinov, A comparative study of hydrazine alternatives in simulated steam generator conditions—Oxygen reaction kinetics and interaction with carbon steel, Electrochim. Acta, 369 (2021) 137697, doi: 10.1016/J.ELECTACTA.2020.137697.

[17] T. Tran, F. Huet, K. Ngo, P. Rousseau, Artefacts in electrochemical impedance measurement in electrolytic solutions due to the reference electrode, Electrochim. Acta, 56 (2011) 8034–8039, doi: 10.1016/j.electacta.2010.12.088.

[18] L. Yu, S. M. Reutzel-Edens, C. A. Mitchell, Crystallization and polymorphism of conformationally flexible molecules: Problems, patterns, and strategies, Org. Process Res. Dev., 4 (2000) 396–402, doi: 10.1021/op000028v.

[19] A. Gavezzotti, G. Filippini, Polymorphic Forms of Organic Crystals at Room Conditions: Thermodynamic and Structural Implications, J. Am. Chem. Soc., 117 (1995) 12299–12305, doi: 10.1021/ja00154a032.

[20] M. R. Caira, Crystalline Polymorphism of Organic Compounds, 198 (1998) 163–208, doi: 10.1007/3-540-69178-2_5.

[21] Q. Zhang, Q. Zhang, L. A. Archer, Molecular relaxation dynamics of self-assembled monolayers, J. Phys. Chem. B, 110 (2006) 4924–4928, doi: 10.1021/jp060259p.

[22] A. K. Jonscher, The ‘universal’ dielectric response, Nature, 267 (1977) 673–679, doi: 10.1038/267673a0.

[23] C. Dyre, T. B. Schrøder, Universality of ac conduction in disordered solids, Rev. Mod. Phys., 72 (2000) 873–892, doi: 10.1103/RevModPhys.72.873.

[24] J. C. Dyre, The random free-energy barrier model for ac conduction in disordered solids, J. Appl. Phys., 64 (1988) 2456–2468, doi: 10.1063/1.341681.

[25] J. Oviedo, M. A. San-Miguel, J. A. Heredia-Guerrero, J. J. Benítez, Electrostatic induced molecular tilting in self-assembled monolayers of n-octadecylamine on mica, J. Phys. Chem. C, 116 (2012) 7099–7105, doi: 10.1021/jp300829g.

[26] S. Chakri, I. Frateur, M. E. Orazem, E. Sutter, M. T. T. Long, B. Tribollet, V. Vivier Improved EIS analysis of the electrochemical behaviour of carbon steel in alkaline solution, Electrochim. Acta, 246 (2017) 924-930, doi: 10.1016/j.electacta.2017.06.096ï.

[27] L. Freire, M. J. Carmezim, M. G. S. Ferreira, M. F. Montemor, The passive behaviour of AISI 316 in alkaline media and the effect of pH: A combined electrochemical and analytical study, Electrochim. Acta, 55 (2010) 6174–6181, doi: 10.1016/j.electacta.2009.10.026.

[28] S. Campen, J. H. Green, G. D. Lamb, H. A. Spikes, In situ study of model organic friction modifiers using liquid cell AFM: Self-assembly of octadecylamine, Tribol. Lett., 58 (2015) 1-15, doi: 10.1007/s11249-015-0514-5.

[29] E. Siurdyban, T. Brotin, K. Heuzé, L. Vellutini, T. Buffeteau, Immobilization of Cryptophane Derivatives onto SiO_2 /Au and Au Substrates, Langmuir, 30 (2014) 14859–14867, doi: 10.1021/la5039156.

[30] H. Yoshioka, K. Yoshida, N. Noguchi, T. Ueki, K. Murai, K. Watanabe, M. Nakahara, Microscopic structure and binding mechanism of the corrosion-protective film of oleylpropanediamine on copper in hot water, J. Phys. Chem. C, 126 (2022) 6436–6447, doi: 10.1021/acs.jpcc.2c00526.

[31] M. Márcio, S. Goés, H. Rahman, J. Ryall, J. J. Davis, P. R. Bueno, A dielectric model of self-assembled monolayer interfaces by capacitive spectroscopy, Langmuir, 28 (2012) 9689−9699, doi: 10.1021/la301281y.

[32] E. R. Dionne, F. Ben Amara, A. Badia, An electrochemical immittance analysis of the dielectric properties of self-assembled monolayers,Can. J. Chem., 98 (2020) 471–479, doi: 10.1139/cjc-2020-0005.

[33] R. Subramanian, V. Lakshminarayanan, Study of kinetics of adsorption of alkanethiols on gold using electrochemical impedance spectroscopy, Electrochim. Acta, 45 (2000) 4501–4509, doi: 10.1016/S0013-4686(00)00512-0.

[34] V. S. Dilimon, G. Fonder, J. Delhalle, Z. Mekhalif, Self-assembled monolayer formation on copper: A real time electrochemical impedance study, J. Phys. Chem. C, 115 (2011) 18202–18207, doi: 10.1021/jp203652y.

[35] V. S. Dilimon, S. Rajalingam, J. Delhalle, Z. Mekhalif, Self-assembly mechanism of thiol, dithiol, dithiocarboxylic acid, disulfide and diselenide on gold: an

electrochemical impedance study, Phys. Chem. Chem. Phys., 15 (2013) 16648, doi: 10.1039/c3cp51804c.

[36] V. S. Dilimon, J. Denayer, J. Delhalle, Z. Mekhalif, Electrochemical and spectroscopic study of the self-assembling mechanism of normal and chelating alkanethiols on copper, Langmuir, 28 (2012) 6857–6865, doi: 10.1021/la300021g.

[37] S. Wang, J. Zhang, O. Gharbi, V. Vivier, M. Gao, M. E. Orazem, Electrochemical impedance spectroscopy, Nat. Rev. Methods Prim., 1 (2021) 41, doi: 10.1038/s43586-021-00039-w.

[38] A. S. Nguyen, N. Caussé, M. Musiani, M. E. Orazem, N. Pébère, B. Tribollet, V. Vivier, Determination of water uptake in organic coatings deposited on 2024 aluminium alloy: Comparison between impedance measurements and gravimetry, Prog. Org. Coatings, 112 (2017) 93–100, doi: 10.1016/j.porgcoat.2017.07.004.

[39] A. Badia, L. Cuccia, L. Demers, F. Morin, R. B. Lennox, Structure and Dynamics in Alkanethiolate Monolayers Self-Assembled on Gold Nanoparticles: A DSC, FT-IR, and Deuterium NMR Study, J. Am. Chem. Soc., 119 (1997) 2682–2692, doi: 10.1021/ja963571t.

[40] R. G. Nuzzo, E. M. Korenic, L. H. Dubois, Studies of the temperature-dependent phase behavior of long chain n-alkyl thiol monolayers on gold, J. Chem. Phys., 93 (1990) 767–773, doi: 10.1063/1.459528.

[41] F. Schreiber, Structure and growth of self-assembling monolayers, Prog. Surf. Sci., 65 (2000) 151–257, doi: 10.1016/S0079-6816(00)00024-1.

[42] L. H. Dubois, B. R. Zegarski, R. G. Nuzzo, Temperature induced reconstruction of model organic surfaces, J. Electron Spectros. Relat. Phenomena, 54–55 (1990) 1143–1152, doi: 10.1016/0368-2048(90)80304-S.

[43] M. E. Orazem, N. Pébère, B. Tribollet, Enhanced Graphical Representation of Electrochemical Impedance Data, J. Electrochem. Soc., 153 (2006) B129-B136, doi: 10.1149/1.2168377.

[44] B. O'Brien, H. Sahalov, P. C. Searson, The temperature dependence of the impedance of alkanethiol self-assembled monolayers, Appl. Phys. Lett., 97 (2010) 043110, doi: 10.1063/1.3469911.

[45] O. Gharbi, M. T. T. Tran, M. E. Orazem, B. Tribollet, M. Turmine, V. Vivier, Impedance Response of a Thin Film on an Electrode: Deciphering the Influence of the Double Layer Capacitance, *ChemPhysChem*, 22 (2021) 1371–1378, doi: 10.1002/cphc.202100177.